Analysis of angular-error uncertainty in planar multiple-loop structures with joint clearances

Xin Li [a,b], Xilun Ding [a], Gregory S. Chirikjian [b,*]

[a] School of Mechanical Engineering & Automation, Beihang University, 37 Xueyuan Road, Beijing, China
[b] Department of Mechanical Engineering, Johns Hopkins University, 3400 N. Charles St., Baltimore, USA

ARTICLE INFO

ABSTRACT

A model for angular errors in multi-loop structures with joint clearances is established. A closed-form solution of the model is obtained. By using optimization methods and geometric methods, the boundaries of the studied angular errors are determined with reduced computation complexity. In a single loop, the same size joint clearances have identical contributions to the angular error; while in the proposed multi-loop design, the position of the multiple-joint also affects the angular error greatly. The probability density functions (pdfs) of the stated closed-loop errors are also analyzed based on the open loop manipulator. The functions approach being Gaussian distributions if there are many joint clearances. A simple method is presented to evaluate the average and the variance of the pdfs. The method is verified by Monte Carlo simulations.

© 2015 Elsevier Ltd. All rights reserved.

1. Introduction

In high precision tasks, accuracy is always of the utmost importance. Several factors that lead to mechanism angular and positional errors include backlash, compliance, manufacturing errors and input errors [1,2], and sometimes the input errors are considered as the largest error source [3]. But the joint clearances should be considered seriously for at least two reasons: In most complex mechanisms, moving parts are connected by many joints with clearances which are necessary and also cannot be eliminated, so the cumulative error is considerable; the mechanism accuracy is still affected by the joint clearances even if the active joints are frozen.

The problem is being studied persistently in a rather wide range. Path-generating accuracy with joint errors was studied by Mallik and Dhande [4] by using a stochastic model in the confidence level of three-sigma. The path generation and transmission quality was investigated by Erkaya and Uzmay [5], and the joint clearance was considered as a virtual link. Pandey and Zhang [6] applied the principle of maximum entropy to compute the error in the trajectory of a serial manipulator. The trajectory curve error of a four bar linkage with joint gaps was also studied by using Lagrange's equation [7]. In order to keep the output error within the desired limits, a tolerance allocation method was proposed by Fenton, Cleghorn and Fu [8]. Tsai and Lai [9,10] explained why multi-loop linkage accuracy is difficult to analyze, and they used the transmission wrench screw and joint twist screw to solve the problem. Furthermore, screw theory was used to calculate the position accuracy with length or joint errors [11,12]. The principle of virtual work was applied to evaluate the clearance influence. Parenti-Castelli and Venanzi [13] proposed a model for clearance-affected pairs. It was effective when inertial forces acting on links have to be considered. Similarly, pose errors in a 3-UPU robot were investigated in [14] and the position error due to clearances with external load was studied by Innocenti [15], and an example of multi-loop manipulator with locked actuators was given. Joint clearances have a side effect on the system dynamic performance. Flores and Lankarani [16] discussed the dynamic behavior model of rigid multibody systems with multiple revolute clearance joints. The dynamic response of dry, lubricated and

---

* Corresponding author.
  E-mail addresses: li.xin@buaa.edu.cn (X. Li), xlding@buaa.edu.cn (X. Ding), gregc@jhu.edu (G.S. Chirikjian).

frictionless clearance joints were studied by Koshy [17], Machado [18], Tian [19], Flores [20] and Muvengei [21], etc. The work has been extended from rigid body to rigid-flexible multibody [22]. A 2-DOF manipulator [23] and a slider-crank mechanism [24–26] have been studied in terms of their dynamic response. Most of these studies need to rely on the force/torque equilibrium conditions even though the problem is focused only on the geometry errors. In fact, the errors exist objectively with or without load or gravity. Venanzi and Parenti-Castelli [27] proposed a new technique where the force acting on the mechanism was not needed and the maximum displacement error caused by clearances can be directly determined. Other methods used for clearance and tolerance analysis include the matrix method [28], the interval approach [29], the direct linearization method [30], Lie group and Lie algebra methods [31] and a method based on the generalized kinematic mapping of constrained plane motions [32,33]. Most of these methods can deal with the output maximum error caused by joint clearances effectively. Wang and Ehmann [34] analyzed the accuracy of a Stewart platform and described the error sensitivity. Ting, Zhu and Watkins [35] showed that the same value joint clearances contributed to the direction error equally in a single loop linkage. The output error of a mechanism distributes in a scope because uncertainty in the joints deviate. Xu and Zhang [36] established stochastic models for several kinds of joints. Similar research on stochastic errors includes Monte Carlo simulation [37] and variance analysis [38]. Zhu and Ting [39] studied the end point position probability density function of open loop mechanisms. The manipulator error propagation is studied by Wang and Chirikjian [40]. It is shown that the errors propagate by convolution on the Euclidean motion group. Additionally, some research on accuracy focuses on specific mechanisms, such as the 3T1R robot [41], a welding robot [42], a Stewart platform [43], the in-situ fabrication of mechanisms [44] and a class of 3-DoF planar robots [45].

For a deployable mechanism, when some moving parts (or actuators) are locked as a structure, the joint clearances still affect the output accuracy. The output accuracy refers to the positional or angular accuracy of a specific component that we are interested in. In this paper, a model of planar multi-loop structure with joint clearances is established. The angular error boundaries of this model are determined by using an optimization method. In order to simplify the multivariate problem, a geometric analysis is performed. The relationship of serial linkage length errors and a single closed loop angular error is investigated. Then the pdf of the multi-loop direction errors can be given approximately. These functions are compared with the Monte Carlo simulation results.

2. Error model

Although a multi-loop structure can be constructed arbitrarily, the extendible support structure (ESS) is preferred as a good example to illustrate the error analysis clearly. The ESS is used to deploy and support the synthetic aperture radar (SAR) panels for a satellite [46]. The pointing direction of the panels should be accurate for better radar images, which is why the method presented below focuses exclusively on orientational errors. The ESS is always a structure with symmetry and can be described in a plane as shown in Fig. 1, which shows a deployed ESS configuration. Link FG is affixed to the satellite and link FD and DE are the inner panel and the outer panel, respectively.

The ESS is a 3-degree-of-freedom mechanism before it becomes a structure with stable triangles, so some joints should be frozen in Fig. 1, and joints H, I and J are chosen to be locked. The nominal directions of the two panels are perpendicular to FG. But if all joints from A to J are with clearances, the pointing directions will deviate from the expected angles. Then the following questions need to be answered. How to obtain the angular errors of the two panels caused by the joint clearances? Which is the greatest error contribution joint? What does the probability distribution of the error look like?

The character and the influence of the locked joints should be studied first. A typical lock mechanism for the space deployable device is shown in Fig. 2. The joint is driven by a torsional spring to deploy the ESS. A pin is connected to link 1 with a torsion spring, too. The pin moves along the hinge surface of link 2 and finally falls into the groove to complete the locking. If there is a clearance, the locked joint can be shown as in Fig. 3.

In Fig. 3, τ_1 is much greater than τ_2, and a force couple is caused by τ_1. Because of the couple, the joint stays at nearly the same certain contact point, which means that the clearance has a very small influence on the locked links. But the deviation of the locked angle as shown in Fig. 4 may lead to new errors.

The equivalent length l_3 of the two links in Fig. 4 can be written as

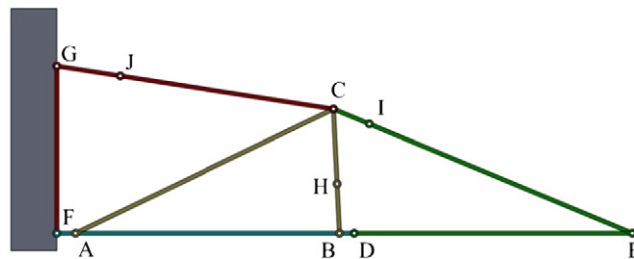$$l_3 = \sqrt{l_1^2 + l_2^2 - 2l_1l_2 \cos(\beta + \Delta\beta)}. \tag{1}$$
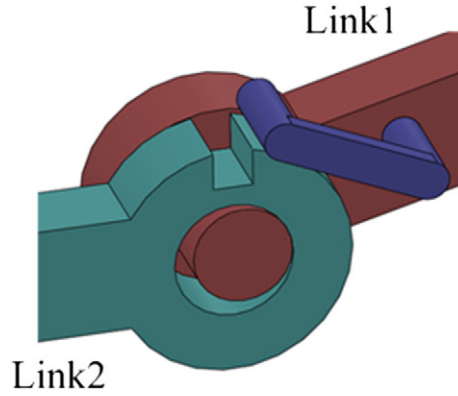

Fig. 1. The support structure.

Fig. 2. The joint lock mechanism.

By using the Taylor Series expansion, the error of l_3 is

$$\Delta l_3 \approx \frac{l_1 l_2 \Delta\beta}{l_3}\sin\beta + \frac{l_1 l_2 (\Delta\beta)^2}{2l_3}\cos\beta. \tag{2}$$

From Fig. 1, we know links BC, CE and CG are all locked with $\beta = \pi$, so the first item of the right side of Eq. (1) is 0 and the second high-order item can be neglected. The locked joints have a very minor influence, so the locked link can be seen as a single object.

We use two models of jointing a hinge. In Fig. 5(a), the pin is fixed at link 1, and the clearance can be represented by a virtual link with length k. In Fig. 5(b), links 1 and 2 share a common pin, and the clearances can be represented by two virtual links.

For the ESS in Fig. 1, to simplify the model, the hinge model type 1 is used for all the joints except joint C. Assume that all of these joints have the same gap size and the pins are in contact with the holes in a relatively stable state. The model can be given as shown in Fig. 6. Such a model is sufficient for analyzing the angular errors of interest in the ESS system. This model is not a simple sum of several triangles, because point B_2 doesn't coincide with point D_2. It will be discussed in the following sections.

The clearances are represented as dashed lines with length k. The angular errors between F_1G_2, F_2D_2 and F_1G_2, D_1E_2 are what we want to study. The middle loop is chosen to be analyzed first. Let F_2D_2 be the fixed link and coordinate A_1-xy is affixed to this link with axis x along A_1B_2. Let lengths of A_1B_2, B_1C_1 and C_2A_2 are l_1, l_2 and l_3, respectively. And the middle loop DoF is

$$F = 3 \times 6 - 2 \times 7 = 4. \tag{3}$$

It equals the numbers of the dashed links in the loop, so the virtual links can move independently. Let the angles between the virtual links and axis x be θ_i ($i = 1, 2, 3, 4$). Points of this loop can be expressed as

$$\mathbf{A}_1 = \begin{bmatrix} 0 & 0 \end{bmatrix}^T \tag{4}$$

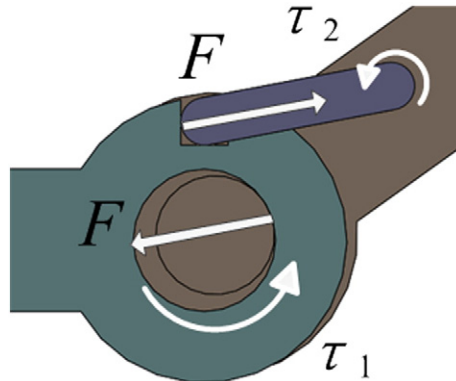$$\mathbf{B}_2 = \begin{bmatrix} l_1 & 0 \end{bmatrix}^T \tag{5}$$
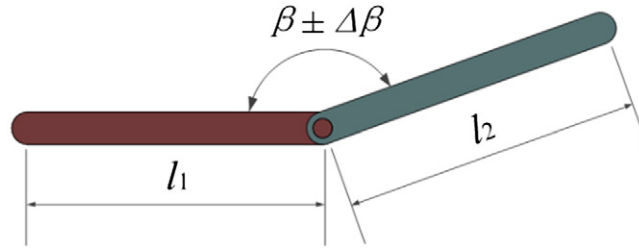

Fig. 3. The locked joint.

Fig. 4. Locking angular deviation.

$$B_1 = B_2 + k[c\theta_1 \quad s\theta_1]^T. \tag{6}$$

Let α_1 denote the angle between B_1C_1 and axis x, so

$$C_1 = B_1 + l_2[c\alpha_1 \quad s\alpha_1]^T \tag{7}$$

$$C_3 = C_1 + k[c\theta_2 \quad s\theta_2]^T \tag{8}$$

$$C_2 = C_3 + k[c\theta_3 \quad s\theta_3]^T \tag{9}$$

$$A_2 = k[c\theta_4 \quad s\theta_4]^T \tag{10}$$

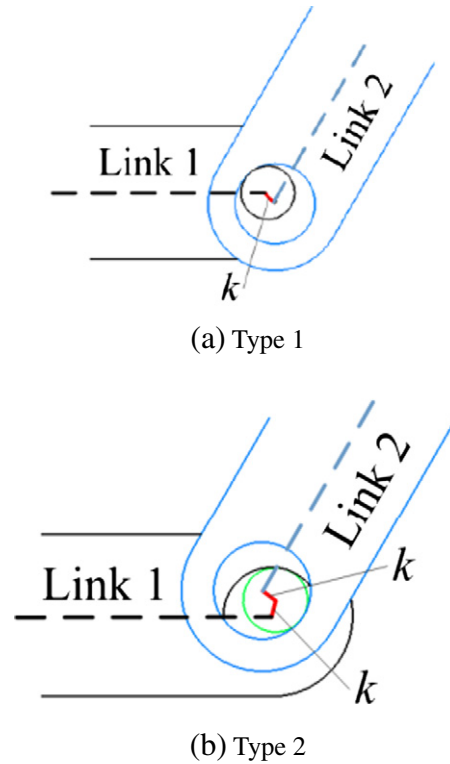where, c and s denote cos and sin, respectively.

(a) Type 1

(b) Type 2

Fig. 5. Hinge configurations.

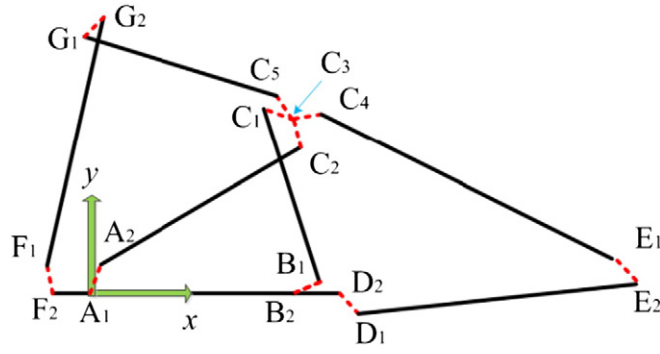**Fig. 6.** Support structure with joint clearances.

According to structural constraints,

$$l_3 - \|A_2C_2\| = 0. \tag{11}$$

Let

$$t_1 = \tan\frac{\alpha_1}{2} \tag{12}$$

then

$$\sin\alpha_1 = \frac{2t_1}{1 + t_1^2}, \quad \cos\alpha_1 = \frac{1 - t_1^2}{1 + t_1^2}. \tag{13}$$

So t_1 can be solved from Eq. (11) as

$$t_1 = \frac{2kl_2b_1 \pm \left[(2l_1l_2 + 2kl_2a_1)^2 - \left(2kl_1a_1 + 2k^2c_1 + d_1\right)^2 + 4k^2l_2^2b_1^2\right]^{\frac{1}{2}}}{2k(l_1 - l_2)a_1 - 2l_1l_2 + 2k^2c_1 + d_1} \tag{14}$$

where,

$$a_1 = \sum_{i=1}^{4} h_i c\theta_i \tag{15}$$

$$b_1 = \sum_{i=1}^{4} h_i s\theta_i \tag{16}$$

$$c_1 = \sum_{j=1}^{3} \sum_{i=j+1}^{4} h_i c\left(\theta_j - \theta_i\right) \tag{17}$$

$$d_1 = l_1^2 + l_2^2 - l_3^2 + 4k^2 \tag{18}$$

$$h_i = \begin{cases} 1, & (i = 1, 2, 3) \\ -1, & (i = 4) \end{cases}. \tag{19}$$

These coefficients need to be adjusted according to the numbers of the clearances. In Eq. (14), there are two solutions for this loop. In the presented configuration, symbol "−" is applied. It can be substituted in Eqs. (4)–(10) to get the point positions. The other two loops can be calculated by using the same model, but one less clearance should be applied. Point C_3 is solved from Eq. (8), and then points A_1 and B_2 can be replaced by points C_3 and D_2 in the right loop. The angle α_2 between D_1E_2 and axis x is obtained accordingly. Similarly, if the angle between F_1G_1 and axis x is denoted as α_3, then replace points C_3 and D_2 with points F_2 and C_3, α_3 can be given. Notice that the configuration of the left triangle loop is different from the other two loops, so symbol "+" will be applied. The angular

error between F_1G_1 and axis x is $\alpha_3 - \pi/2$ and the angular error propagation between F_1G_1 and D_1E_2 is $\alpha_3 - \alpha_2 - \pi/2$. The process is summarized as shown in Fig. 7. It is shown that the constraint coupling problem of the multi-loop structure is totally solved.

3. The extreme angular errors

3.1. Model analysis

The extreme angular errors of the two panels and the error contribution of each joint clearance will be discussed in this section. It is an optimization problem to get the maximum errors. In coordinate A_1-xy, the maximum (minimum) value of the right angular error (panel D_1E_2) α_2 can be computed from

$$\begin{aligned} &\max \text{error}_R = \alpha_2(\theta_1, \theta_2, \ldots, \theta_7) \\ &s.t. \quad 0 \le \theta_i < 2\pi (i = 1, 2, \ldots, 7). \end{aligned} \tag{20}$$

And the angular error between F_1G_1 and D_1E_2 is

$$\begin{aligned} &\max \text{error} = \alpha_3(\theta_1, \ldots, \theta_4, \theta_8, \ldots, \theta_{10}) - \alpha_2(\theta_1, \theta_2, \ldots, \theta_7) - \frac{\pi}{2} \\ &s.t. \quad 0 \le \theta_i < 2\pi (i = 1, 2, \ldots, 10) \end{aligned} \tag{21}$$

where, θ_i is the direction of each joint clearance.

In fact, they are unconstraint optimization problems since θ_i can be with any value. However, there are seven variables in Eq. (20) and ten variables in Eq. (21). Although it is claimed that the single-loop method in reference [35] can be extended to some multi-loop mechanisms, it needs to be discussed further. A single loop structure with joint clearances is shown in Fig. 8.

The angle we care about is γ, and an equivalent model is as shown in Fig. 9.

To find the maximum γ, two possible configurations should be investigated, as shown in Fig. 10.

Calculate

$$\cos\gamma_{1\max} - \cos\gamma_{2\max} = \frac{l_1^2 + l_2^2 - (l_3 + K)^2}{2l_1 l_2} - \frac{(l_1 - K)^2 + l_2^2 - l_3^2}{2(l_1 - K)l_2} = \frac{K(K - l_1 + l_2 + l_3)(K - l_1 - l_2 + l_3)}{2l_1 l_2(l_1 - K)} < 0 \tag{22}$$

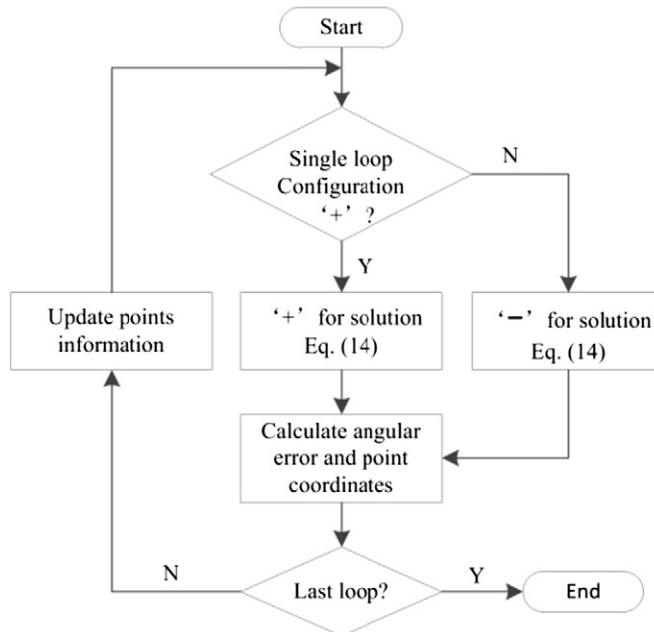where, $K = k_1 + k_2 + k_3$, then

$$\gamma_{1\max} > \gamma_{2\max}. \tag{23}$$

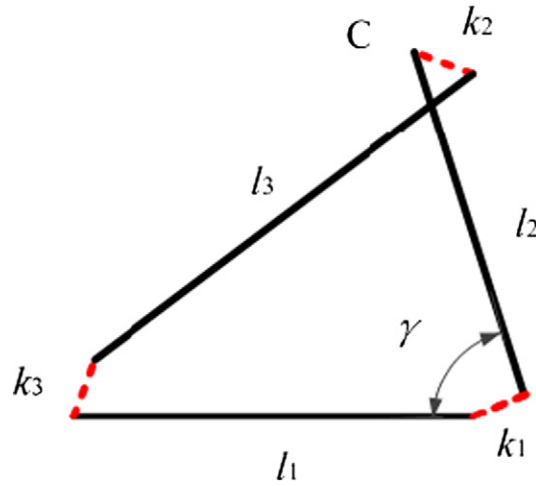**Fig. 7.** Error computation process for multi-loop structure.

Fig. 8. Single loop with clearances.

So in configuration A, γ reaches its peak value, and all the clearance directions can be known immediately.

However, as mentioned in the last section, the multi-loop structure is not a simple sum of single loops. For example, in Fig. 11, by maximizing $\angle P$, $\angle Q$ doesn't reach its minimum. This is because when B_1C_1 rotates anticlockwise, the distance between C_3 and D_2 may become longer, and as a result, $\angle P$ may tend to be smaller.

For the above reason, the stated geometric method can only be used in the outermost single loop. But it should still reduce the computational complexity. In Eqs. (20) and (21), the variable numbers go down from seven and ten to four. Also, there is another way to make the calculation much easier, as shown in Fig. 12.

Curves N_1N_3 and N_2N_4 are sections of the circles with center at A_1 (in Fig. 11) and radii equal to $l_{A2C2} \pm 2\,k$; while curves N_1N_2 and N_3N_4 are sections of the circles with center at B_2 and radii equal to $l_{B1C1} \pm 2\,k$. Point C_3 must lie in the shadow area. These curves can be seen as four straight lines which are easy to be determined. So Eq. (21) can be expressed as

$$\begin{aligned} &\max \text{error} = f(\mathbf{C}_3) \\ &s.t. \quad \mathbf{C}_3 \text{ in the shadow area.} \end{aligned} \tag{24}$$

Accordingly, the minimal values of these errors can be given. Although the joint clearances affect the angular error equally, their contributions to the displacement of position C_3 are different, as shown in Fig. 13.

In Fig. 13, each joint gap is removed individually. Point T_3 coincides with point T_2, which means clearances k_2 and k_3 have the same effect, while k_1 and k_2 are not. The difference is shown in Fig. 13(b) and the nominal point T is shown in Fig. 13(a). In the presented triangles, the horizontal displacement of T is affected more by k_1 while the vertical displacement is affected more by k_2.
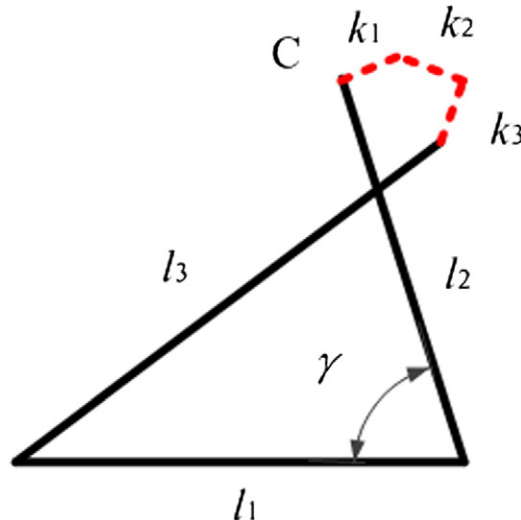

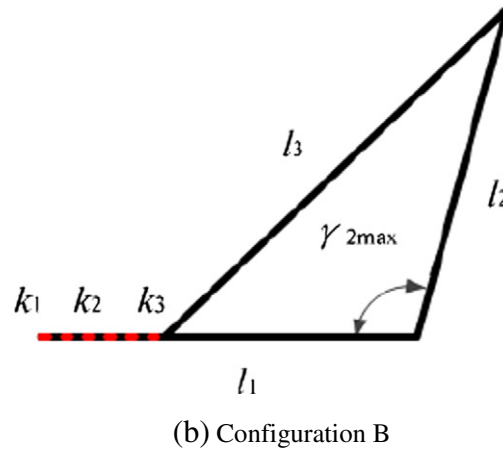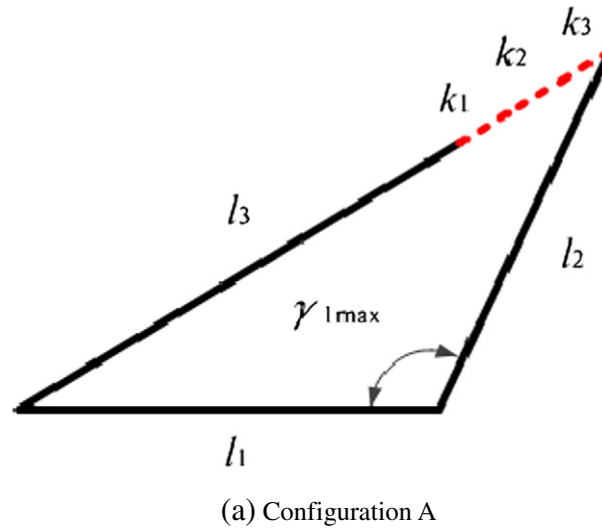Fig. 9. Equivalent single loop with clearances.

(a) Configuration A

(b) Configuration B

Fig. 10. Two possible configurations of maximum angle.

3.2. Numerical example

A numerical example is given according to the derivation above. The example parameters are listed in Table 1.

According to the analysis of the last subsection, the boundaries of some angular errors in coordinate A_1-xy are summarized in Table 2 with the corresponding point C_3, where, the first three errors are as defined at the end of Section 2, and the error sum is $[\alpha_2^2 + (\alpha_3 - \pi/2)^2]^{1/2}$. The direction parallel to the x axis is defined as 0.
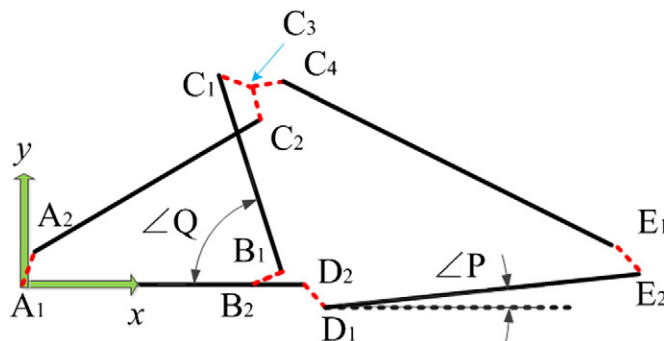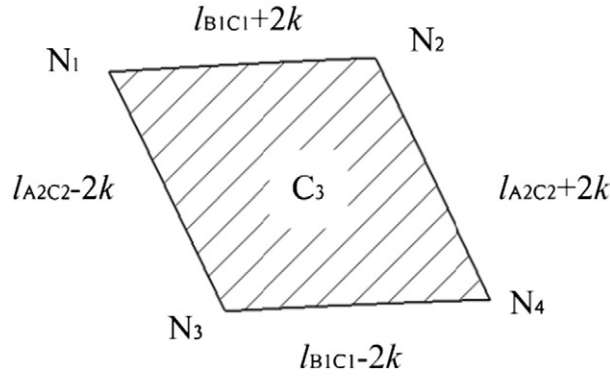

Fig. 11. Explanation of multi-loop angular error.

Fig. 12. Area of point C_3.

4. Probability distribution functions of angular errors

The error propagation problem with pdf analysis of open loop mechanisms has been studied by convolution on the Euclidean motion group, $SE(n)$ [40,47,48]. As pointed out in these references, if an open loop manipulator is separated into two segments with error workspace densities of $\rho_1(g)$ and $\rho_2(g)$, $g = (R,\mathbf{x}) \in SE(n)$, convolving the densities results in the density for the whole manipulator. The joint positional and orientational density for the two segments' manipulator will be

$$\rho_{1,2}(R, \mathbf{x}) = \int_{A \in SO(n)} \int_{\mathbf{y} \in R^n} \rho_1(A, \mathbf{y}) \rho_2 \left(A^T R, A^T (\mathbf{x} - \mathbf{y}) \right) dA d\mathbf{y} \tag{25}$$

where, dA is the Haar measure for $SO(n)$ and $d\mathbf{y}$ is the Lebesgue measure for R^n.

It is already complicated. In addition, the closed loop structures are even more difficult to analyze because of coupling constraints. In Fig. 14, the length of l_3 with clearances k should be studied first.

Obviously, the length is an open loop problem, since the clearance is small enough, a simpler way can be found, since $(k\sin\eta_1)^2$ is a negligible high order item, then

$$l_{31} = \sqrt{(l_3 + k\cos\eta_1)^2 + (k\sin\eta_1)^2} \approx l_3 + k\cos\eta_1. \tag{26}$$

If there are more joint gaps, then

$$l_{3n} \approx l_3 + k\sum_{i=1}^{n} \cos\eta_i. \tag{27}$$

In the space environment, it is reasonable to assume that the clearance angle η_i distributes uniformly. So the pdf is

$$\rho_{\eta i} = \frac{1}{2\pi}, \quad \eta_i \in [0, 2\pi). \tag{28}$$

The cumulative distribution function of $\cos\eta_1$ is

$$\begin{aligned} P(\cos\eta_1 \leq X) &= P(\arccos X \leq \eta_1 \leq 2\pi - \arccos X) = P(\eta_1 \leq 2\pi - \arccos X) - P(\eta_1 \leq \arccos X) \\ &= 1 - \frac{\arccos X}{\pi}, \quad X \in [-1, 1]. \end{aligned} \tag{29}$$

So,

$$\rho_{\cos\eta_1} = P'(\cos\eta_1 \leq X) = \frac{1}{\pi\sqrt{1 - X^2}}. \tag{30}$$

Let $a_i = \cos\eta_i$, then

$$P(a_1 + a_2 \leq X) = P(a_2 \leq X - a_1) = \int_{-\infty}^{+\infty} \int_{-\infty}^{X - a_1} \rho_{a_1 a_2}(a_1, a_2) da_1 da_2 \tag{31}$$
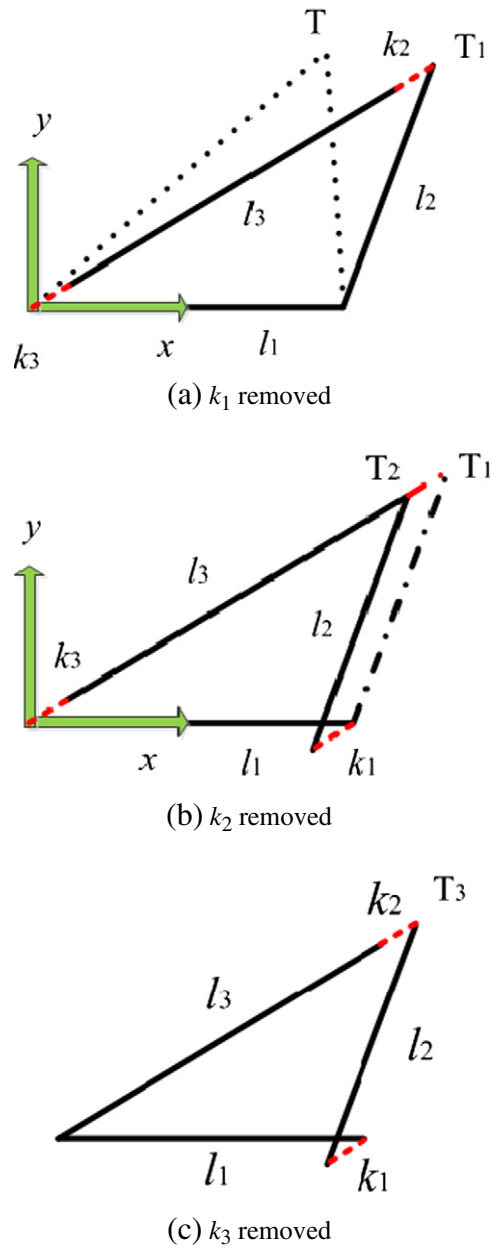
(a) k_1 removed

(b) k_2 removed

(c) k_3 removed

Fig. 13. Position effects of joint clearances.

Table 1
Structure parameters (mm).

Middle loop	A_1B_2	B_1C_1	A_2C_2
	198	93	214.67
Right loop	B_2D_2	D_1E_2	E_1C_4
	11	208	242
Left loop	A_1F_2	F_1G_2	G_1C_5
	14	125	210
Clearances	k		
	0.5		

Table 2
Angular error boundaries.

	Right error α_2	Left error $\alpha_3 - \pi/2$	Error propagation	Error sum
Maximum (*rad*)	0.0407	0.0257	0.0403	0.0482
C_3 (*mm, mm*)	N_1 (191.98, 93.81)	N_1 (191.98, 93.81)	N_4 (195.08, 91.95)	N_1 (191.98, 93.81)
Minimum (*rad*)	-0.0417	-0.0257	-0.0393	0.0011
C_3 (*mm, mm*)	N_4 (195.08, 91.95)	N_4 (195.08, 91.95)	N_1 (191.98, 93.81)	(193.84, 92.50)

so,

$$\rho_{a_1+a_2}(X) = \int_{-\infty}^{+\infty} \rho_{a_1}(a_1)\rho_{a_2}(X-a_1)\,da_1 = \frac{1}{\pi^2}\int_{-1}^{1}\frac{1}{\sqrt{1-a_1^2}}\cdot\frac{1}{\sqrt{1-(X-a_1)^2}}\,da_1 \tag{32}$$

or expressed in convolution form,

$$\rho_{a_1+a_2}(X) = \rho_{\cos\eta_1} * \rho_{\cos\eta_2}(X) \tag{33}$$

and,

$$\rho_{a_1+a_2+\ldots+a_n}(X) = \rho_{\cos\eta_1} * \rho_{\cos\eta_2} * \cdots * \rho_{\cos\eta_{l_n}}(X). \tag{34}$$

Infinity spikes in these functions in small intervals make sense. For example, Eq. (30) is infinity when $X = \pm 1$, but its integral can be expressed as Eq. (29).

Eq. (32) is an improper integral, and we will have trouble in solving it even by using numerical methods, not to mention Eq. (34). However, according to the Lindeberg–Levy central limit theorem, Eq. (34) will approach the Gaussian distribution when $n \to \infty$. The average and variance of a_i are

$$\mu_i = \mu = \int_{-1}^{1}\frac{a_i}{\pi\sqrt{1-a_i^2}}\,da_i = 0 \tag{35}$$

$$\sigma_i^2 = \sigma^2 = \int_{-1}^{1}\frac{a_i^2}{\pi\sqrt{1-a_i^2}}\,da_i = \frac{1}{2}. \tag{36}$$
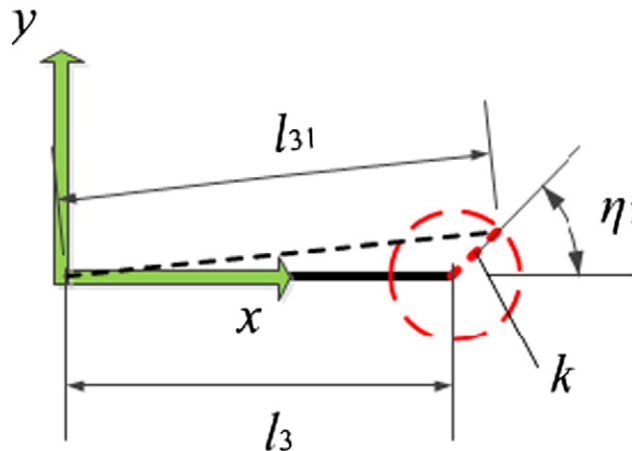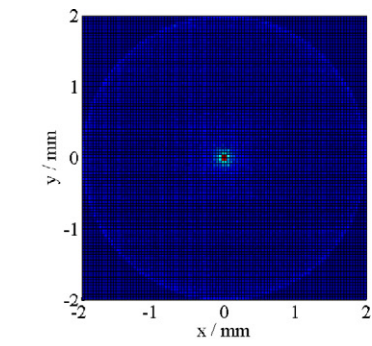
Let

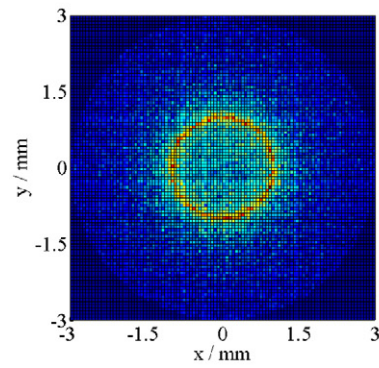$$a_\Sigma = \sum_{i=1}^{n} a_i \tag{37}$$
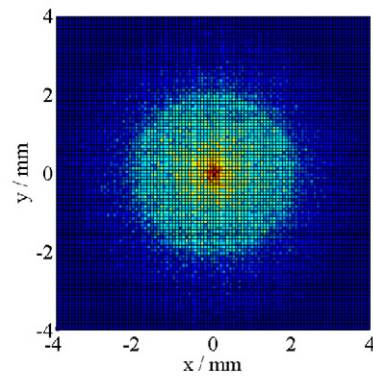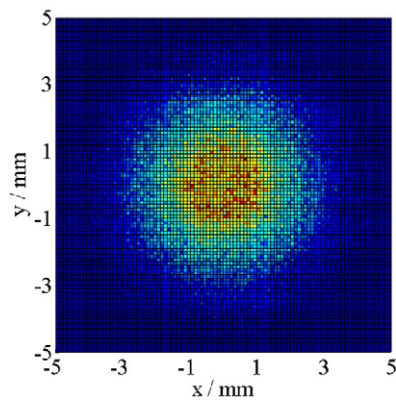

Fig. 14. The equivalent length with clearance.

(a) *n=2*

(b) *n=3*

(c) *n=4*

(d) *n=5*

Fig. 15. Monte Carlo simulation frequency.

then

$$\rho_{a_1+a_2+\ldots+a_n}(X) \approx \frac{1}{\sqrt{2n\pi}\sigma} e^{\frac{-a_\Sigma^2}{2n\sigma}}. \tag{38}$$

Monte Carlo simulations are conducted when n equals 2 to 5 (10^5 times for each). The frequency of each point is plotted in Fig. 15. In the electronic version of this paper, the color code goes from blue to red, with red denoting high frequency.

According to the simulations of Fig. 15, further study shows that when $n \geq 5$, Eq. (38) is close enough to a Gaussian distribution. When $n = 5$, taking the parameters listed in Table 1, Eq. (27) can be seen as a convergence in distribution to

$$\rho_{l_{3n}} \sim N\left(l_3, 5k^2\sigma^2\right) = N(214.670.625). \tag{39}$$

The pdf is compared with the Monte Carlo simulation result in Fig. 16.

The following analysis is for the closed loop angular errors, based on the open loop conclusions above. If the pdf ρ_x is known, and $y = f(x)$, then

$$\rho_y(Y) = \rho_x\left(f^{-1}(Y)\right)\left|\frac{df^{-1}(Y)}{dY}\right|. \tag{40}$$

As shown in Figs. 8 or 9, let $b = \cos\gamma$, so,

$$l_{3n} = \sqrt{l_1^2 + l_2^2 - 2l_1 l_2 b}. \tag{41}$$

According to Eq. (40),

$$\rho_{\cos\gamma}(b) = \rho_{l_{3n}}\left(\sqrt{l_1^2 + l_2^2 - 2l_1 l_2 b}\right)\frac{l_1 l_2}{\sqrt{l_1^2 + l_2^2 - 2l_1 l_2 b}} \tag{42}$$

and,

$$\rho_\gamma(\gamma) = \rho_{\cos\gamma}(\cos\gamma)\sin\gamma. \tag{43}$$

Again, since the joint clearances are very small, γ changes slightly, so

$$\rho_\gamma(\gamma) \approx \frac{l_1 l_2 \sin\gamma_0}{l_3}\rho_{l_{3n}}\left(\sqrt{l_1^2 + l_2^2 - 2l_1 l_2 \cos\gamma}\right) \tag{44}$$

where, γ_0 is the nominal value of γ, or expressed as

$$\gamma_0 = \arccos\frac{\sqrt{l_1^2 + l_2^2 - l_3^2}}{2l_1 l_2}. \tag{45}$$

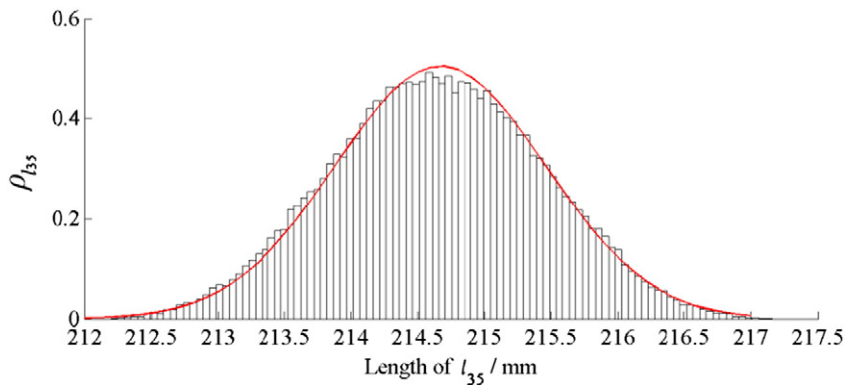The result of Eq. (44) is plotted in Fig. 17 with the simulation density.

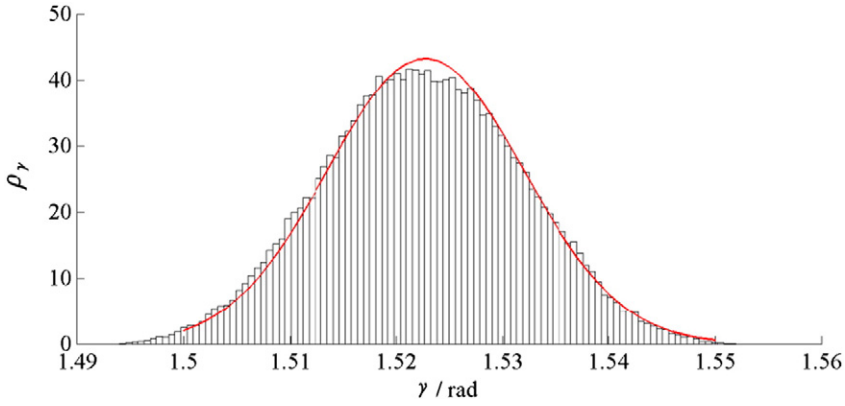Fig. 16. Comparison of the pdf and simulation for l_{35}.

Fig. 17. Comparison of the pdf and simulation for γ ($n = 5$).

It still looks like a Gaussian distribution, but it can't be explained by Eq. (44). We need to find another way to explain the curve directly. In fact, we have

$$\gamma = \arccos \frac{l_1^2 + l_2^2 - (l_3 + k a_{\sum})^2}{2 l_1 l_2} \tag{46}$$

and

$$\gamma \approx \gamma_0 + \frac{l_3 k + k^2 a_{\sum}}{l_1 l_2 \sqrt{1 - \left(\frac{l_1^2 + l_2^2 - (l_3 + k a_{\sum})^2}{2 l_1 l_2}\right)^2}} . \tag{47}$$

Ignoring small items, obtain

$$\gamma \approx \gamma_0 + \frac{l_3 k}{l_1 l_2 \sin \gamma_0} a_{\sum} . \tag{48}$$

So Eq. (44) can be replaced by

$$\rho_\gamma \sim N\left(\gamma_0, \left(\frac{l_3 k}{l_1 l_2 \sin \gamma_0}\right)^2 n \sigma^2\right) = N\left(1.5228, 8.51 \times 10^{-5}\right). \tag{49}$$

While the average and variance of the simulation in Fig. 17 are 1.5228 and 8.50×10^{-5}, respectively, they are nearly the same.

The above analysis is suitable for single closed-loop structure with any number of joint clearances. But the Gaussian distribution can only be used when the number is equal to or greater than 5. However, multiple joints are more often used than single joints, so there are at least 6 clearances even in a three-joint-triangle structure.

For the multi-loop structure in Fig. 1, the angular error $\Delta\gamma\_R$ between DE and axis x is mainly affected by $\angle CBA$ and $\angle CDE$. To make it simpler, we can ignore the error caused by the positional errors, and just investigate how the joint clearances (four independent joint clearances in the middle triangle and three in the right triangle) affect $\Delta\gamma\_R$ independently. The sum of the seven errors can be seen approximately as $\Delta\gamma\_R$. Again, by using Monte Carlo simulation, we know that the error approaches a Gaussian distribution, then according to the Lindeberg–Feller central limit theorem,
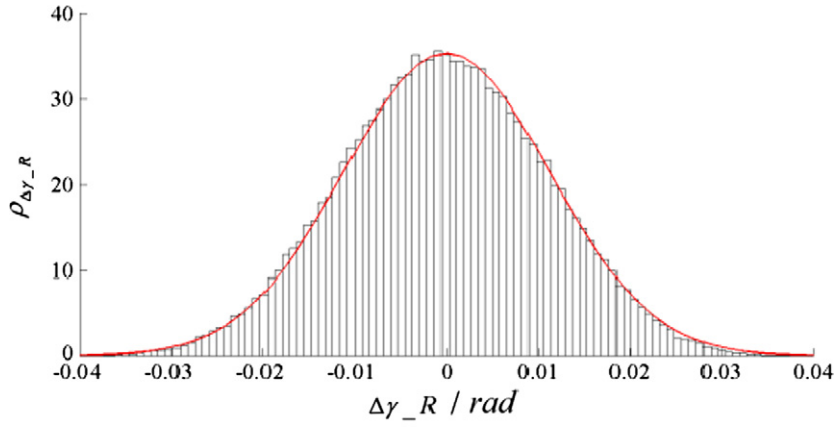
$$\rho_{\Delta\gamma\_R} \sim N\left(0, 4\left(\frac{l_3 k}{l_1 l_2 \sin \gamma_0}\right)^2 \sigma^2 + 3\left(\frac{l_6 k}{l_4 l_5 \sin \gamma_{R0}}\right)^2 \sigma^2\right) = N\left(0, 1.27 \times 10^{-4}\right) \tag{50}$$

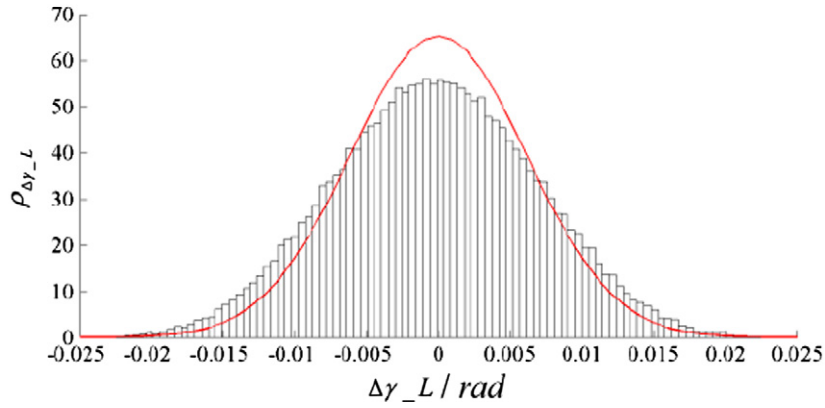where, l_4, l_5 and l_6 denote the lengths of CD, DE and CE and γ_{R0} denotes the nominal value of $\angle CDE$.

Similarly, $\Delta\gamma\_L$ denoting the angular error between FG and axis y is

$$\rho_{\Delta\gamma\_L} \sim N\left(0, 3.74 \times 10^{-5}\right). \tag{51}$$

They are both plotted in Fig. 18 with the simulation results.

(a) Right angular error

(b) Left angular error

Fig. 18. Angular errors for multi-loop structure.

The analysis for the multi-loop errors is not as good as that for the single-loop because the model has been simplified. Because $l_{CD} < l_{CF}$, point C_3 has a smaller effect in the right loop, that is the reason why Fig. 18(a) is much more accurate than Fig. 18(b). However, it is not necessary to make any simulations to obtain the pdf roughly.
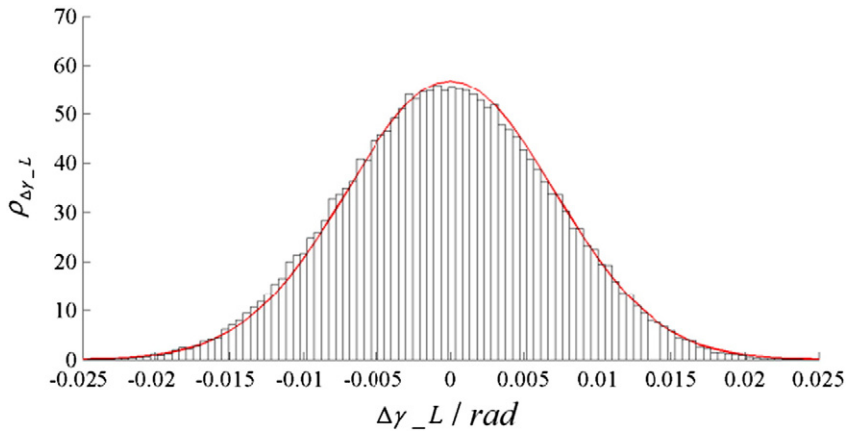
Fig. 19. Modified left angular error.

To make the analysis more accurate, Monte Carlo simulations for the middle triangle are needed. In fact, $\Delta\gamma\_L$ is caused by the clearances of the left ΔGFC and point C_3. They can be seen as two independent parts. Let $C_3 = (C_x, C_y)$, in Fig. 1, $\Delta\gamma\_L$ caused by point C_3 only is

$$e_1 = \arccos\frac{l_{GF}^2 + l_{FC}^2 - l_{CG}^2}{2l_{GF}l_{FC}} + \arctan\frac{C_y}{C_x + l_{FA}} - \frac{\pi}{2} \tag{52}$$

where,

$$l_{FC} = \sqrt{(C_x + l_{FA})^2 + C_y^2}. \tag{53}$$

By the Monte Carlo simulation, we get $\mathrm{var}(e_1) = 2.4780 \times 10^{-5}$.

According to Eq. (49), the variance of the error caused by the ΔGFC (triangle lengths change very small) is 2.4574×10^{-5}. In Eq. (50), the pdf of $\Delta\gamma\_L$ can be modified as

$$\rho_{\Delta\gamma\_L} \sim N\left(0, 2.4780 \times 10^{-5} + 2.4574 \times 10^{-5}\right) = N\left(0, 4.9354 \times 10^{-5}\right). \tag{54}$$

Accordingly, Fig. 18(b) is modified as in Fig. 19.

The difference between Figs. 18(b) and 19 is mainly caused by the position of C_3. The pdf of the errors that caused this point is difficult to determine, so the Monte Carlo simulation method is used. However, only the simulation for the middle loop is enough to estimate the errors of the multi-loop structure. In Fig. (19), compared to the bar chart, the computational work to generate the curve is reduced nearly by half.

5. Conclusions

The angular errors for a multi-loop structure with joint clearances are studied in this paper systematically. The model of clearances for single joint, multi-joint and locked joint are presented. Accordingly, the explicit solutions for the multi-loop angular errors are obtained. Then the boundaries of the errors are investigated by using the optimization method. The joint clearance geometry configurations are studied to explain and to simplify the optimization problems. It is shown that the angular errors of the end loops are affected by the angular and positional errors together of the middle loop, and in the end loop, the same size joint clearances contribute to the angular error identically. In the presented structure, the optimization variables are reduced to four from seven (two loops) and ten (three loops), respectively. The analysis of probability density function is extended to deal with the multiple closed-loop structure. The studied errors are distributed according to the Gaussian distribution. All of the analyses are verified by using the Monte Carlo simulations.

Acknowledgment

References

[1] S. Briot, I.A. Bonev, Accuracy analysis of 3-DOF planar parallel robots, Mech. Mach. Theory 43 (2008) 445–458.
[2] G. Chen, H. Wang, Z. Lin, A unified approach to the accuracy analysis of planar parallel manipulators both with input uncertainties and joint clearance, Mech. Mach. Theory 64 (2013) 1–17.
[3] J. Merlet, Computing the worst case accuracy of a PKM over a workspace or a trajectory, The 5th Chemnitz Parallel Kinematics Seminar 2006, pp. 83–96 (Chemnitz, Germany, Citeseer).
[4] A.K. Mallik, S.G. Dhande, Analysis and synthesis of mechanical error in path-generating linkages using a stochastic approach, Mech. Mach. Theory 22 (1987) 115–123.
[5] S. Erkaya, I. Uzmay, Determining link parameters using genetic algorithm in mechanisms with joint clearance, Mech. Mach. Theory 44 (2009) 222–234.
[6] M.D. Pandey, X. Zhang, System reliability analysis of the robotic manipulator with random joint clearances, Mech. Mach. Theory 58 (2012) 137–152.
[7] R. Mishra, T. Naskar, S. Acharya, Synthesis of coupler curve of a four bar linkage with joint clearances, Synthesis 3 (2013) 1193–1199.
[8] R. Fenton, W. Cleghorn, J.-f. Fu, Allocation of dimensional tolerances for multiple loop planar mechanisms, J. Mech. Des. 111 (1989) 465–470.
[9] M.J. Tsai, T.H. Lai, Accuracy analysis of a multi-loop linkage with joint clearances, Mech. Mach. Theory 43 (2008) 1141–1157.
[10] M.J. Tsai, T.H. Lai, Kinematic sensitivity analysis of linkage with joint clearance based on transmission quality, Mech. Mach. Theory 39 (2004) 1189–1206.
[11] U. Kumaraswamy, M. Shunmugam, S. Sujatha, A unified framework for tolerance analysis of planar and spatial mechanisms using screw theory, Mech. Mach. Theory 69 (2013) 168–184.
[12] A. Frisoli, M. Solazzi, D. Pellegrinetti, M. Bergamasco, A new screw theory method for the estimation of position accuracy in spatial parallel manipulators with revolute joint clearances, Mech. Mach. Theory 46 (2011) 1929–1949.
[13] V. Parenti-Castelli, S. Venanzi, Clearance influence analysis on mechanisms, Mech. Mach. Theory 40 (2005) 1316–1329.
[14] A.H. Chebbi, Z. Affi, L. Romdhane, Prediction of the pose errors produced by joints clearance for a 3-UPU parallel robot, Mech. Mach. Theory 44 (2009) 1768–1783.
[15] C. Innocenti, Kinematic clearance sensitivity analysis of spatial structures with revolute joints, J. Mech. Des. 124 (2002) 52–57.
[16] P. Flores, H.M. Lankarani, Dynamic response of multibody systems with multiple clearance joints, J. Comput. Nonlinear Dyn. 7 (2012) (031003-031003).

[17] C.S. Koshy, P. Flores, H.M. Lankarani, Study of the effect of contact force model on the dynamic response of mechanical systems with dry clearance joints: computational and experimental approaches, Nonlinear Dyn. 73 (2013) 325–338.
[18] M. Machado, J. Costa, E. Seabra, P. Flores, The effect of the lubricated revolute joint parameters and hydrodynamic force models on the dynamic response of planar multibody systems, Nonlinear Dyn. 69 (2012) 635–654.
[19] Q. Tian, Y. Sun, C. Liu, H. Hu, P. Flores, ElastoHydroDynamic lubricated cylindrical joints for rigid–flexible multibody dynamics, Comput. Struct. 114–115 (2013) 106–120.
[20] P. Flores, H. Lankarani, Spatial rigid-multibody systems with lubricated spherical clearance joints: modeling and simulation, Nonlinear Dyn. 60 (2010) 99–114.
[21] O. Muvengei, J. Kihiu, B. Ikua, Numerical study of parametric effects on the dynamic response of planar multi-body systems with differently located frictionless revolute clearance joints, Mech. Mach. Theory 53 (2012) 30–49.
[22] C. Liu, Q. Tian, H. Hu, Dynamics and control of a spatial rigid-flexible multibody system with multiple cylindrical clearance joints, Mech. Mach. Theory 52 (2012) 106–129.
[23] L.X. Xu, Y.G. Li, Investigation of joint clearance effects on the dynamic performance of a planar 2-DOF pick-and-place parallel manipulator, Robot. Comput. Integr. Manuf. 30 (2014) 62–73.
[24] P. Flores, C. Koshy, H. Lankarani, J. Ambrósio, J.C.P. Claro, Numerical and experimental investigation on multibody systems with revolute clearance joints, Nonlinear Dyn. 65 (2011) 383–398.
[25] P. Flores, J. Ambrósio, Revolute joints with clearance in multibody systems, Comput. Struct. 82 (2004) 1359–1369.
[26] Z. Zhang, L. Xu, P. Flores, H.M. Lankarani, A Kriging model for dynamics of mechanical systems with revolute joint clearances, J. Comput. Nonlinear Dyn. 9 (2014) 310–319.
[27] S. Venanzi, V. Parenti-Castelli, A new technique for clearance influence analysis in spatial mechanisms, J. Mech. Des. 127 (2005) 446–455.
[28] P.D. Lin, J.F. Chen, Accuracy analysis of planar linkages by the matrix method, Mech. Mach. Theory 27 (1992) 507–516.
[29] W. Wu, S. Rao, Interval approach for the modeling of tolerances and clearances in mechanism analysis, J. Mech. Des. 126 (2004) 581–592.
[30] J.W. Wittwer, K.W. Chase, L.L. Howell, The direct linearization method applied to position error in kinematic linkages, Mech. Mach. Theory 39 (2004) 681–693.
[31] J. Meng, D. Zhang, Z. Li, Accuracy analysis of parallel manipulators with joint clearance, J. Mech. Des. 131 (2009) 011013.
[32] G. Chen, H. Wang, Z. Lin, Generalized kinematic mapping of constrained plane motions and its application to the accuracy analysis of general planar parallel robots, Mech. Mach. Theory 50 (2012) 29–47.
[33] G. Chen, H. Wang, Z. Lin, A unified approach to the accuracy analysis of planar parallel manipulators both with input uncertainties and joint clearance, Mech. Mach. Theory 64 (2013) 1–17.
[34] S.M. Wang, K.F. Ehmann, Error model and accuracy analysis of a six-DOF Stewart platform, J. Manuf. Sci. Eng. 124 (2002) 286–295.
[35] K.L. Ting, J. Zhu, D. Watkins, The effects of joint clearance on position and orientation deviation of linkages and manipulators, Mech. Mach. Theory 35 (2000) 391–401.
[36] W.L. Xu, Q.X. Zhang, Probabilistic analysis and Monte Carlo simulation of the kinematic error in a spatial linkage, Mech. Mach. Theory 24 (1989) 19–27.
[37] J.H. Choi, S.J. Lee, D.H. Choi, Stochastic linkage modeling for mechanical error analysis of planar mechanisms, J. Struct. Mech. 26 (1998) 257–276.
[38] S. Lee, B. Gilmore, The determination of the probabilistic properties of velocities and accelerations in kinematic chains with uncertainty, J. Mech. Des. 113 (1991) 84–90.
[39] J. Zhu, K.L. Ting, Uncertainty analysis of planar and spatial robots with joint clearances, Mech. Mach. Theory 35 (2000) 1239–1256.
[40] Y. Wang, G.S. Chirikjian, Error propagation on the Euclidean group with applications to manipulator kinematics, Robotics IEEE Trans. 22 (2006) 591–602.
[41] S. Briot, I.A. Bonev, Accuracy analysis of 3T1R fully-parallel robots, Mech. Mach. Theory 45 (2010) 695–706.
[42] S. Erkaya, Investigation of joint clearance effects on welding robot manipulators, Robot. Comput. Integr. Manuf. 28 (2012) 449–457.
[43] T. Ropponen, T. Arai, Accuracy analysis of a modified Stewart platform manipulator, Robotics and Automation, 1995, Proceedings, 1995 IEEE International Conference on, IEEE 1995, pp. 521–525.
[44] S. Rajagopalan, M. Cutkosky, Error analysis for the in-situ fabrication of mechanisms, J. Mech. Des. 125 (2003) 809–822.
[45] A. Yu, I.A. Bonev, P. Zsombor-Murray, Geometric approach to the accuracy analysis of a class of 3-DOF planar parallel robots, Mech. Mach. Theory 43 (2008) 364–375.
[46] W.D. Thomas, RADARSAT-2 extendible support structure, Can. J. Remote. Sens. 30 (2004) 282–286.
[47] G.S. Chirikjian, A.B. Kyatkin, Engineering applications of noncommutative harmonic analysis: with emphasis on rotation and motion groups, CRC press, 2000.
[48] H. Dong, Z. Du, G.S. Chirikjian, Workspace density and inverse kinematics for planar serial revolute manipulators, Mech. Mach. Theory 70 (2013) 508–522.